ELSEVIER

Temporal evolution and geochemical variability of the South Pacific superplume activity

Alain Bonneville [a,*], Laure Dosso [b], Anthony Hildenbrand [c]

[a] Institut de Physique du Globe de Paris 4, Place Jussieu, 75252 Paris Cedex 05, France
[b] Centre National de la Recherche Scientifique, UMR 6538 IFREMER, BP 70, 29280 Plouzané, France
[c] Centre National de la Recherche Scientifique, Laboratoire Géochronologie, Université Paris-Sud, 91405 Orsay, France

Abstract

We are presenting a new set of K/Ar ages and geochemical analyses obtained on deep-sea samples dredged in 1999 on several seamounts of the Cook–Austral volcanic chains in the Pacific Ocean. The new geochemical results, together with published data on island samples, allow us to reveal a time evolution of the mantle source composition as well as an increase in geochemical variability of the superplume responsible for the regional South Pacific Superswell. Three identified volcanic stages of 58–40, 33–20 and 20–0 Ma are identified with signatures of mantle reservoir composition varying from close to C to N-MORB-types and C/HIMU-type, respectively. Using a geodynamic reconstruction for the most recent volcanic period, from 20 Ma to present, three hotspot tracks are needed to explain the several volcanic episodes observed within the limited geographical area of the central part of the Cook–Austral chains. At the scale of a single volcano, different magmatic phases can also be identified with different ages and geochemical signatures, emphasizing the importance of structural control, either crustal or lithospheric, in the location of the magmatic outputs. These observations, taken together, are in good agreement with a model where each hotspot could sample a small volume of the large very heterogeneous plume responsible for the regional South Pacific Superswell.
© 2006 Elsevier B.V. All rights reserved.

1. Introduction

The Cook–Austral volcanic chain is located on the southern part of the Pacific plate, in a region of anomalous shallow seafloor known as the South Pacific Superswell [1]. This region of anomalously high bathymetry is also geochemically anomalous and known as the location of the South Pacific Isotope and Thermal Anomaly, SOPITA [2]. The Cook–Austral

chain signature, based essentially on island sampling, is often attributed to a "HIMU"-type mantle source characterized by Mid-Ocean Ridge Basalt (MORB) — like Sr isotopic ratios and highly radiogenic Pb isotopic ratios (see review in [3]). Deep-sea samples of the Austral chain were collected during the ZEPOLYF2 cruise that took place in July 1999 between 22°S and 28°S latitude and 143°W and 155°W longitude (Figs. 1 and 2). Geophysical data including multibeam bathymetry, acoustic imagery, seismic reflection, gravity and magnetic data were also collected. 31 seamounts were mapped and 24 dredges recovered volcanoclastic

---

* Corresponding author. Tel.: +33 1 44 27 68 94; fax: +33 1 44 27 99 69.
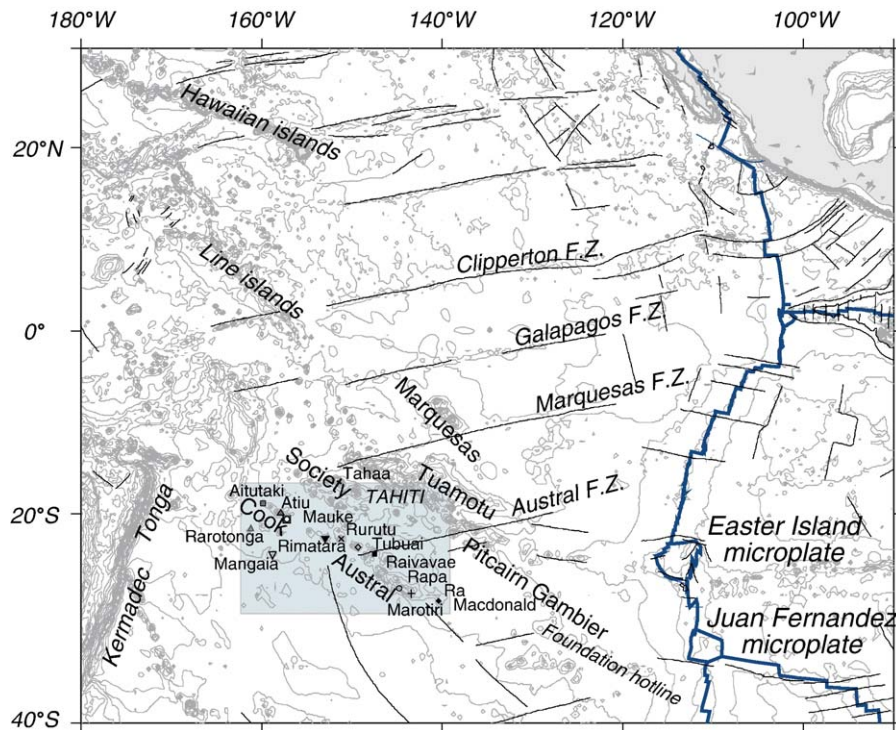 E-mail address: bonneville@ipgp.jussieu.fr (A. Bonneville).

Fig. 1. Location of the Cook–Austral Islands in the southwest Pacific with indication of the main structural features and names of main sampled islands. The box corresponds to the studied area displayed in Fig. 2.

sediments, altered and fresh pillow basalts, hyaloclastites and ferromanganese crusts. We present here geochemical data obtained on 17 samples selected from these dredges on the basis of their petrographic freshness. Two additional basaltic samples were included in this study (PLD07 and PLD09, Fig. 2); they were collected in March 1998 during the POLYDRAG1 cruise (chief scientist, A. Bonneville) on the Tarava Seamount chain located between the Society island and the Austral island chains [4]. This collection of submarine basalt samples has been dated by K/Ar techniques. These new geochemical results, together with published data on island samples, allow us to explore the link between the volcanic activity observed at the Earth surface and deep mantle processes.

2. Geological setting

The Cook–Austral chain extends from the island of Aitutaki (140°W, 29°S) to the active submarine volcano Macdonald (160°W, 19°S) in a band more than 2200 km long and 240 km wide, oriented N115°E (Figs. 1 and 2). The chain is composed of several dozens of seamounts and of 11 islands and 2 atolls with little area above sea level (70 km^2 for the largest island). The Austral

Fracture Zone (FZ) cuts the chain between the islands of Tubuai and Raivavae. Although oriented roughly in the direction of present Pacific plate motion (11 cm y^{-1} along a N115° direction), the spatial and temporal pattern of both the aerial and submarine volcanoes is rather complex.

The age of the oceanic crust along the chain ranges from about 39 to 84 Ma [5] (Fig. 2). Several K/Ar or Ar/Ar ages are available on almost all the islands of the Cook–Austral chain and on seamounts in the Taukina and Ngatemato seamount chains [6], but to date no seamount in the northern Austral region has been dated yet.

The particular geometry and morphology of the chain have suggested so far two distinct but parallel alignments [7]. In 1997, McNutt et al. [6] determined the existence of two additional chains of volcanoes near the active Macdonald seamount at the southeast end of the chain, 20–34 m.y. older than the Macdonald volcanism. Both recent and old ages recorded on Aitutaki, and Rurutu islands basaltic samples [8,9] suggest the existence of two other hotspots (Rarotonga and Rurutu) and in 2002, Bonneville et al. [10] proposed that the most recent volcanic stage of Rurutu be attributed to Arago Seamount, a very shallow seamount
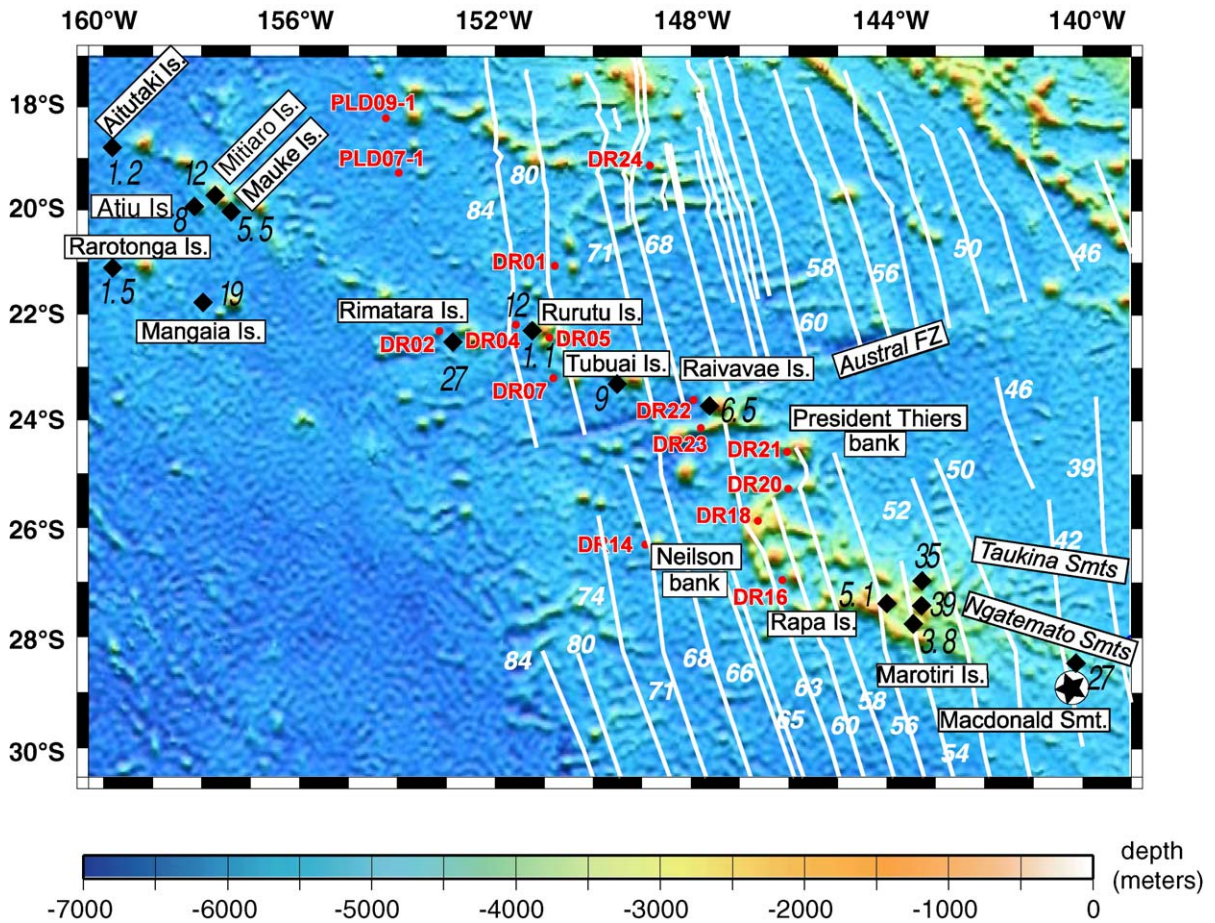
Fig. 2. Ages of seafloor and island volcanoes reported on a shaded view of seafloor topography for the Cook–Austral region. The 34j anomaly (84 Ma) marks the beginning of the Cretaceous quiet zone and west of this anomaly (∼ longitude 152°W), the crust has an age comprised between 84 and 118 Ma. White lines represent crustal magnetic anomalies, and their corresponding age is in white numbers (Ma). Black diamonds represent places where K–Ar or Ar/Ar ages (Ma, in black italic) are known. Dredge location and sample numbers are in red.

located 120 km east-southward of Rurutu and sampled during the ZEPOLYF2 cruise. To summarize, up to 6 distinct hotspot tracks have been identified so far: from northwest to southeast, Rarotonga, Arago, Tubuai, Macdonald, Taukina and Ngatemato of which three are probably still active, Rarotonga, Arago and Macdonald.

3. K–Ar dating of the dredged samples

During the ZEPOLYF2 cruise, 24 successful dredges were performed (Fig. 2). Most of them were on lava flows covering the seamount slopes and most of them are very altered. They are classical pillow basalts with a major glassy phase in which the microlitic content increases towards the core. They contain some early crystallized phenocrysts, often altered, with inherited radiogenic Argon in various proportions. They also contain secondary mineral phases like zeolites due to fluid circulation. Moreover, right or immediately after the emplacement of the flow, the matrix is devitrified yielding to formation of mainly clay minerals.

Some basaltic samples have a very low K and high Ca content. Despite the low K, K/Ar method remains the most appropriate one to date basalts younger than 60 Ma, if applied to a mineral phase representative of the lava flow emplacement [11–13]. Our samples contain different mineral assemblages corresponding to the successive stages of the lava history: (1) evolution in the magma chamber, (2) solidification on the seafloor, (3) hydrothermal circulation and finally, (4) in situ alteration. The chronometer is, thus, very questionable, and the whole rock dating of such lavas is unsuitable.

Even though $^{40}Ar/^{39}Ar$ technique allows a distinction between phases to be made using a step heating procedure on whole rock grains [13], we chose to work with a single phase technique. The selection of the correct phase is critical to get the age of the lava flow, i.e. stage (2). This phase in our samples is generally microlitic plagioclase and occasionally nepheline. The rapid cooling of the pillow-basalt, however, limits the size of these microlites to some tens of microns. This small size precludes the use of the $^{40}Ar/^{39}Ar$ dating technique because of the recoil of ^{39}Ar during the neutron activation. Moreover, the very high Ca content of plagioclase restricts the applicability of $^{40}Ar/^{39}Ar$ dating technique, especially for younger rocks for which the radiogenic ^{40}Ar content is very low. Considering these limitations, we decided to use a K–Ar dating technique devoted to detect very low radiogenic ^{40}Ar contents: the Cassignol technique [12,14]. This technique has been previously applied successfully to

submarine basalts from various settings, and yielded ages coherent with the stratigraphic and geodynamic constraints [4].

3.1. Sample preparation

The inner part of the pillows is systematically used for dating. A specific technique is applied to extract the pure microlitic plagioclase phase when preserved. First, the rocks are crushed and sieved to a 125 to 500 μm size fraction. Heavy liquids are used to remove all phenocrysts and to select the pure microlitic groundmass. Then, the groundmass is crushed again to a smaller size such as to isolate pure plagioclase microlites (generally around 30 to 50 μm). Finally, a magnetic separator is used to separate pure plagioclase from the altered glass and other microlites. The different microlitic sizes extracted from the various samples are summarized in Table 1. When possible, different

Table 1
Results of the K–Ar dating

Sample	Phase	Range of crystal sizes (μm)	K%	$^{40}Ar*$ (%)	$^{40}Ar*$ (at/g)	Age (Ma)	Uncertainty
DR01	Plagioclase	125–250	0.199	71.13	1.2357E+13	58.5	0.8
DR01	Plagioclase	125–250	0.199	72.56	1.2171E+13	57.6	0.8
				Mean		58.1	0.8
DR02	Groundmass	125–250	0.826	6.86	2.2481E+12	2.57	0.05
DR02	Groundmass	125–250	0.826	6.23	2.3029E+12	2.63	0.06
				Mean		2.60	0.05
DR04	Groundmass	125–250	0.909	70.48	1.1813E+13	12.2	0.2
DR04	Groundmass	125–250	0.909	65.96	1.1865E+13	12.3	0.2
				Mean		12.2	0.2
DR05	Plagioclase	80–125	0.333	69.34	1.9481E+13	55.2	0.8
DR05	Plagioclase	80–125	0.333	70.58	1.9256E+13	54.5	0.8
				Mean		54.8	0.8
DR07	Nepheline	125–250	2.818	12.68	6.7574E+11	0.230	0.004
DR07	Groundmass	125–250	1.558	1.27	2.0809E+10	0.013	0.002
DRO7B	Plagioclase	50–80	0.623	28.27	5.8006E+12	8.89	0.13
DR07Bfd	Plagioclase	125–250	0.251	34.96	2.0267E+12	7.71	0.11
				Mean		8.24	0.65
DR14-03	Groundmass	125–250	1.128	61.91	1.0340E+13	8.76	0.13
DR14-03	Groundmass	125–250	1.128	47.11	1.0398E+13	8.80	0.13
				Mean		8.78	0.13
DR16-01	Plagioclase	125–250	0.377	56.00	1.5735E+13	39.5	0.6
DR16-01	Plagioclase	125–250	0.377	55.48	1.5735E+13	39.5	0.6
				Mean		39.5	0.6
DR18-02	Plagioclase	125–250	0.224	50.25	6.6699E+12	28.3	0.4
DR18-02	Plagioclase	125–250	0.224	42.78	6.5168E+12	27.6	0.4
				Mean		28.0	0.4
DR23-02	Plagioclase	125–250	0.146	47.17	5.1964E+12	33.3	0.5
DR23-02	Plagioclase	50–80	0.271	30.66	9.2456E+12	31.9	0.5
				Mean		32.7	0.5
DR24-02	Plagioclase	40–80	1.215	7.28	1.3293E+13	10.4	0.3
DR24-02	Plagioclase	40–80	1.215	17.10	1.3367E+13	10.5	0.2
				Mean		10.5	0.2

mineral phases are isolated: plagioclase microlites, plagioclase phenocrysts, nepheline (Fig. 3) and ground-mass. They constitute independent phases which are important to check for internal consistency of a given sample. This is illustrated in pillow-lavas DR07B and DR24-02 (Fig. 4) for which both plagioclase crystals (125–250 μm) and microlites (30–50 μm) have been separated and analyzed.
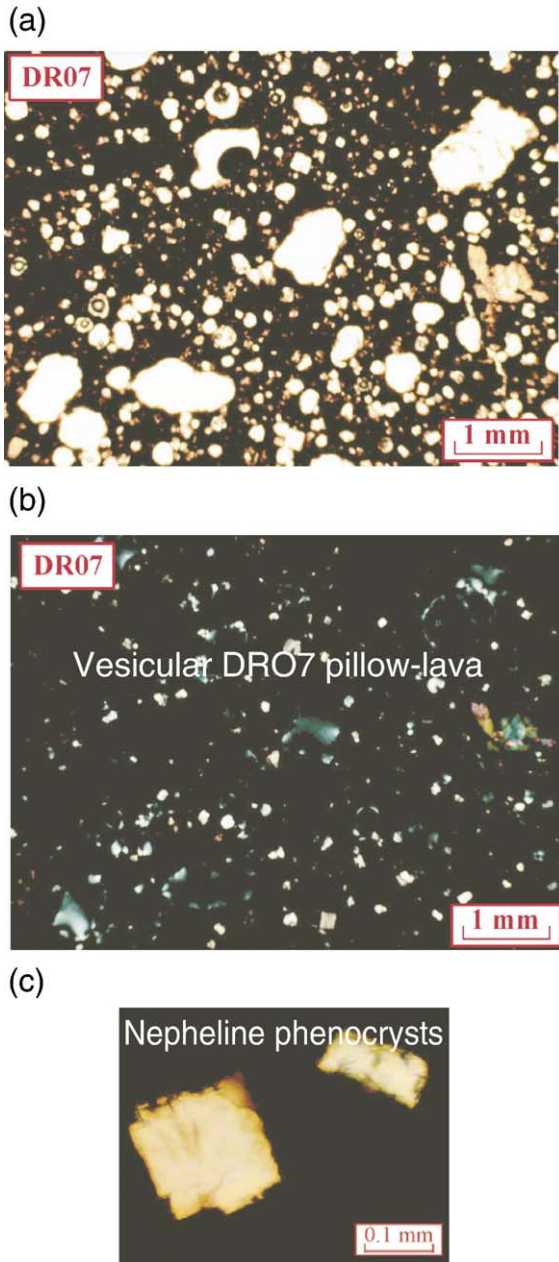
(a)

(b)

(c)

Fig. 3. (a) and (b) DR07 pillow lava observed in thin section. (c) Nepheline phenocrysts can be observed within the vesicular altered groundmass.

(a)
Crushing and sieving at 200 μm - 400 μm

Separation of the microlitic groundmass

(b)
Crushing and sieving at 40 μm - 80 μm

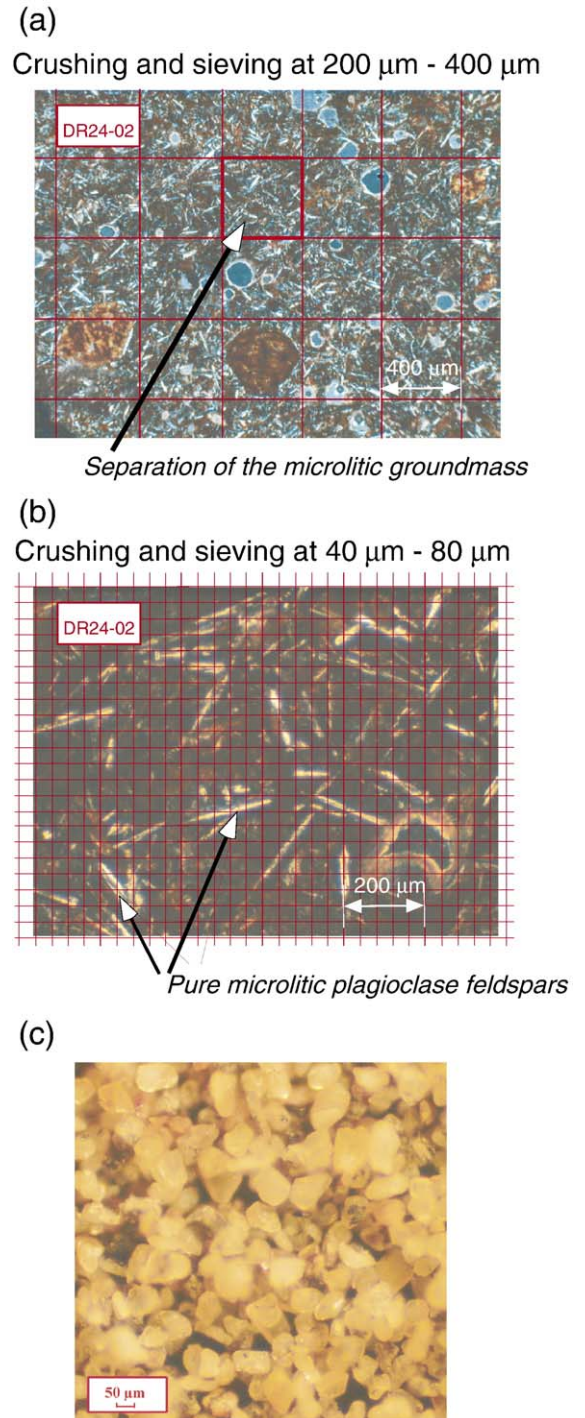Pure microlitic plagioclase feldspars

(c)

Fig. 4. Extraction of the microlitic plagioclase from DR24-02 basalt, using the double separation technique: (a) crushing at an appropriate size to remove unsuitable phenocrysts; (b) re-crushing and sieving at a smaller size to extract the plagioclase microlites (c).

Table 2
Major, trace element and isotopic composition of analyzed samples

Sample	DR01-7	DR01-8	DR02-1	DR02-2	DR04-2	DR05-1	DR07
Lat. S	20°42.9	20°42.9	22°28.8	22°28.8	22°20.4	22°33.8	23°25.5
Long. W	150°50.2	150°50.2	153°6.7	153°6.7	151°31.7	151°2.3	150°44.7
Seamount	ZEP2-1	ZEP2-1	ZEP2-12	ZEP2-12	ZEP2-7	Lotus	Arago
Summit depth (m)	1050	1050	300	300	1350	450	26.5
Age (Ma)	58.1	58.1	2.6	2.6	12.2	54.8	0.23
SiO_2	46.44	46.97	44.07	43.84	46.29	40.78	39.36
Al_2O_3	15.89	15.19	15.35	12.79	14.77	17.81	15.49
Fe_2O_3	13.56	12.50	13.04	12.70	13.25	14.86	13.86
FeO							
MnO	0.09	0.11	0.18	0.16	0.16	0.11	0.24
MgO	4.17	4.80	6.24	8.61	4.48	0.95	5.8
CaO	7.63	9.29	13.24	14.11	11.22	10.22	10.83
Na_2O	3.40	3.48	2.92	2.60	3.55	3.66	7
K_2O	1.24	1.04	0.80	0.69	1.19	0.86	1.47
TiO_2	3.05	2.83	3.12	2.83	3.86	3.36	2.65
P_2O_5	0.82	0.87	0.46	0.49	0.53	2.98	0.97
LOI (1050 °C)	3.38	2.72	0.93	0.85	0.90	3.59	0.68
Total	99.67	99.80	100.35	99.67	100.20	99.18	98.37
Th (0.085)	0.965	0.917	4.48	3.99	4.29	1.29	16.76
La (0.687)	15.40	15.17	35.01	29.38	25.62	21.77	117.83
Nb (0.713)	17.79	16.12	50.97	35.06	51.49	21.46	129.79
Ta (0.041)	1.29	1.20	3.68	2.36	3.60	1.63	8.91
Ce (1.775)	38.36	37.37	72.40	66.15	59.79	46.66	216.88
Pr (0.276)	5.40	5.32	8.79	8.37	7.65	6.65	23.17
Nd (1.354)	26.61	25.78	36.04	33.74	33.56	31.24	87.11
Zr (11.2)	252.8	228.9	213.6	185.0	275.0	270.3	362.9
Hf (0.309)	5.61	5.16	4.61	4.14	6.02	5.79	6.39
Sm (0.444)	7.86	7.29	7.80	7.76	7.51	8.32	15.15
Eu (0.168)	2.51	2.47	2.65	2.35	2.72	3.01	4.55
Gd (0.596)	8.34	8.11	6.82	6.12	7.11	8.68	12.44
Tb (0.108)	1.28	1.23	0.94	0.88	1.00	1.27	1.64
Dy (0.737)	7.23	6.91	5.18	4.65	5.38	7.16	8.15
Y (4.55)	39.45	37.94	27.14	23.41	26.96	41.86	39.61
Ho (0.164)	1.40	1.34	0.93	0.85	0.93	1.31	1.34
Er (0.480)	3.61	3.53	2.37	2.10	2.34	3.43	3.11
Tm (0.074)	0.5116	0.5249	0.3341	0.2672	0.3161	0.499	0.3836
Yb (0.493)	3.28	3.10	1.93	1.53	1.82	3.03	2.17
Lu (0.074)	0.50	0.47	0.29	0.23	0.27	0.45	0.30
$^{143}Nd/^{144}Nd$	0.512928	0.512791	0.512912	0.512927	0.512872	0.512953	0.512918
$^{87}Sr/^{86}Sr$	0.703040	0.703048	0.702613	0.702989	0.702884	0.703167	0.703371
$^{206}Pb/^{204}Pb$	18.387	18.483	20.333	20.256	20.872	18.636	20.459
$^{207}Pb/^{204}Pb$	15.531	15.531	15.658	15.652	15.749	15.534	15.708
$^{208}Pb/^{204}Pb$	37.940	38.049	39.953	39.792	40.185	37.981	39.978

Major and trace element composition analyzed by XRF (Brest), ICP-MS (C.R.P.G. Nancy) and *microprobe (Brest)* when in italic. All Sr isotopic measurements are obtained with $2\sigma_M$ errors of less than 20 and Nd measurements are obtained with $2\sigma_M$ errors of less than 15. Pb isotope measurements are done by double spike technique (see text). Normalization values used to present the data in the extended rare earth patterns of Fig. 6 are given in parenthesis after the element name. Ages are K–Ar dates from Table 1 or estimated when shown in italic.

DR07-2	DR07B	DR14-3	DR14-4	DR16-1	DR18-3	DR18B gl	DR18D gl	DR18G gl
23°25.5	23°25.5	26°23.7	26°23.7	27°1.4	25°49.7	25°49.7	25°49.7	25°49.7
150°44.7	150°44.7	148°55.8	148°55.8	146°10.0	146°18.3	146°18.3	146°18.3	146°18.3
Arago	Arago	ZEP2-19	ZEP2-19	Neilson	ZEP2-26	ZEP2-26	ZEP2-26	ZEP2-26
26.5	26.5	600	600	3	1250	1250	1250	1250
0.23	8.2	8.8	?	39.5	28.0	28.0	28.0	28.0
46.82	44.13	48.15	48.97	44.51	44.12	47.68	*47.78*	47.15
17.27	17.6	12.49	4.99	16.31	18.39	16.48	*15.57*	16.15
13.05	13.14	9.26	5.80	12.66	13.48	12.31		12.30
							4.46	
0.21	0.1	0.11	0.08	0.09	0.16	0.15	*0.193*	0.18
4.15	1.81	7.43	15.18	3.64	1.76	5.42	*6.631*	6.78
8.61	9.15	13.83	21.78	10.01	9.11	9.02	*10.15*	9.95
5.29	3.61	2.82	0.49	3.02	3.11	3.25	*3.35*	3.27
1.30	1.49	1.29	0.06	1.47	1.04	0.83	*0.40*	0.46
2.64	3.46	3.05	1.57	3.32	2.64	2.56	*2.57*	2.46
0.62	1.71	0.47	0.03	1.10	1.72	0.36	*0.35*	0.31
0.26	2.51	0.71	0.46	3.35	3.23	1.16		0.85
100.22	98.71	99.61	99.41	99.48	98.76	99.22	*100.68*	99.86
6.32	6.59	4.08	0.201	2.28	0.726	0.633		0.707
45.54	49.22	25.91	6.25	32.00	13.93	9.99		10.42
65.00	64.27	35.92	2.76	37.85	10.97	11.35	12.0	11.04
4.72	4.81	2.81	0.24	2.73	0.84	0.86		0.81
94.23	102.24	59.07	15.38	69.45	32.48	28.22		29.39
11.03	11.94	7.50	2.67	9.16	4.91	3.99		4.44
44.70	46.35	31.11	13.68	38.38	23.01	18.60		19.80
254.5	290.4	221.3	62.7	279.2	213.8	223.3	221	218.9
5.35	6.82	5.65	2.50	6.48	5.09	5.17		4.90
8.64	9.28	6.95	3.89	8.32	6.40	5.19		5.86
2.63	2.90	2.24	1.33	2.63	2.20	1.76		1.86
7.51	7.95	6.40	3.88	7.99	7.16	5.78		6.45
1.08	1.08	0.86	0.54	1.10	1.08	0.88		1.02
6.28	6.23	4.81	2.72	5.77	6.81	5.47		6.22
32.16	34.55	21.99	11.34	32.71	40.89	30.99	29.1	34.33
1.16	1.16	0.85	0.44	1.13	1.38	1.08		1.24
2.96	2.81	2.07	0.98	2.95	4.03	2.92		3.26
0.4277	0.4113	0.2572	0.1189	0.3998	0.5909	0.4138		0.4819
2.69	2.65	1.60	0.67	2.48	3.62	2.78		3.18
0.40	0.41	0.21	0.09	0.36	0.52	0.42		0.48
0.512927	0.512940	0.512687	0.512908	0.512944	0.513132	0.513115	0.513137	0.513125
0.703215	0.703350	0.704338	0.702763	0.703029	0.702603	0.702576	0.702621	0.702674
20.430	19.842	18.952	19.452	18.784	18.219	18.173	18.101	18.084
15.705	15.604	15.617	15.608	15.574	15.477	15.485	15.465	15.473
39.966	39.495	38.997	39.239	38.167	37.477	37.501	37.452	37.468
		18.951						
		15.618						
		39.002						

Table 2 (*continued*)

Sample	DR20-2 gl	DR21-2	DR22	DR23-2 gl	DR23-3	PLD07-1	PLD09-1
Lat. S	25°15.0	24°32.8	23°46.9	24°10.5	24°10.5	19°27.2	18°58.1
Long. W	145°40.3	145°50.1	147°29.0	147°49.0	147°49.0	153°54.7	154°6.9
Seamount	ZEP2-31	Pdt Thiers	NE flank Raivavae	SW flank Raivavae	SW flank Raivavae	Titi	Fafa Piti
Summit depth (m)	1450	19	19	2950	2950	979	799
Age (Ma)	>20	?	?	32.7	?	?	43.5
SiO_2	48.00	37.12	45.34	47.60	42.14	34.46	44.59
Al_2O_3	15.74	13.44	13.41	16.24	18.18	14.12	17.11
Fe_2O_3	11.42	18.41	13.59	12.68	12.02	13.28	11.10
FeO							
MnO	0.17	0.24	0.17	0.17	0.13	0.13	0.05
MgO	8.40	7.21	10.85	7.72	2.48	0.89	3.59
CaO	11.13	13.56	9.16	9.46	11.76	15.72	9.02
Na_2O	3.08	1.42	2.42	2.66	2.66	3.17	3.38
K_2O	0.15	0.83	1.19	0.61	1.11	1.18	1.69
TiO_2	1.47	4.76	1.97	1.55	2.31	3.77	2.46
P_2O_5	0.14	0.55	0.19	0.14	2.63	7.38	2.61
LOI (1050 °C)	-0.57	2.48	2.41	1.41	3.99	3.80	3.70
Total	99.13	100.02	100.70	100.24	99.41	97.90	99.31
Th (0.085)	0.191		1.68	0.257	3.871	1.555	1.138
La (0.687)	3.42		14.44	4.12	54.05	27.66	47.45
Nb (0.713)	2.90	99.8	22.06	3.83	47.40	26.14	19.35
Ta (0.041)	0.22		1.62	0.30	3.70	1.96	1.43
Ce (1.775)	10.43		32.39	13.31	58.24	59.90	48.92
Pr (0.276)	1.71		4.01	1.89	9.80	7.97	7.69
Nd (1.354)	9.17		16.91	9.48	41.90	35.81	33.06
Zr (11.2)	91.8	275	120.0	106.8	194.9	283.8	189.1
Hf (0.309)	2.33		2.98	2.55	4.64	6.12	4.44
Sm (0.444)	3.25		4.06	2.93	7.55	9.24	7.25
Eu (0.168)	1.30		1.39	1.08	2.50	3.21	2.47
Gd (0.596)	4.20		4.11	3.69	7.83	9.02	7.90
Tb (0.108)	0.68		0.62	0.62	1.13	1.32	1.11
Dy (0.737)	4.49		3.49	4.05	7.01	7.39	6.61
Y (4.55)	26.98	52.3	19.67	23.25	55.17	47.86	62.14
Ho (0.164)	0.94		0.67	0.88	1.45	1.42	1.41
Er (0.480)	2.52		1.71	2.38	4.01	3.55	3.86
Tm (0.074)	0.3966		0.2479	0.385	0.5646	0.5392	0.5699
Yb (0.493)	2.54		1.56	2.47	3.94	3.31	3.50
Lu (0.074)	0.38		0.23	0.37	0.64	0.48	0.54
$^{143}Nd/^{144}Nd$	0.513151	0.512825	0.512912	0.513081	0.512963	0.512921	0.512802
$^{87}Sr/^{86}Sr$	0.702595	0.702763	0.702919	0.702650	0.703139	0.703036	0.703072
$^{206}Pb/^{204}Pb$	17.589	20.168	19.835	17.991	20.270	19.082	18.782
$^{207}Pb/^{204}Pb$	15.476	15.725	15.618	15.490	15.662	15.580	15.542
$^{208}Pb/^{204}Pb$	37.100	39.951	39.426	37.496	39.591	38.148	38.180
				17.992			
				15.491			
				37.501			

Note that the double separation is not necessary for the freshest samples DR02, DR04 and DR14-03, because their groundmass is fresh and well preserved. Finally, special attention has been given to the highly under-saturated glassy pillow-lava DR07 which contains small cubic crystals of nepheline. For this sample, dating has been done both on this particularly K-rich phase and on the preserved glassy groundmass, since the separated nepheline quantities were small.

Most samples have been dated twice and Table 1 summarizes the results:

- for samples with duplicate dates on the same mineral phase (DR01, DR02, DR04, DR05, DR14, DR16, DR18, DR24), ages are perfectly reproducible;
- for DR23 and DR07B, a slight discrepancy can be observed between the dating made on two different phases: (1) microlites and (2) plagioclase phenocrysts;
- for DR07, the dating made on the nepheline phase and on the groundmass are different (by 0.2 Ma) but they are coherent. Both give a very recent age for the sample; however the age based on the nepheline phase is preferred because of the higher K content and of the lower Ar contamination level.

In a few cases very different ages are obtained within a single dredge. This indicates that different volcanic episodes have been sampled along the dredge haul. This can be seen in particular for DR07 and suspected for DR14 and DR23 (see below).
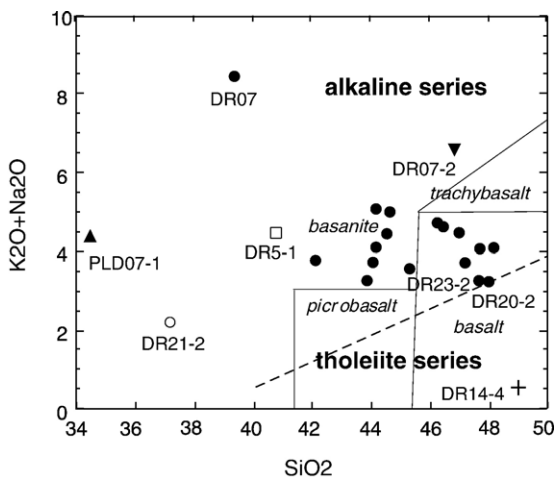
Fig. 5. SiO_2 vs. $Na_2O + K_2O$ for Table 2 data. The field boundaries are from [27] and [28] for the dashed line. DR14-4 is a basaltic breccia rich in clinopyroxenes shown by a slashed circle.
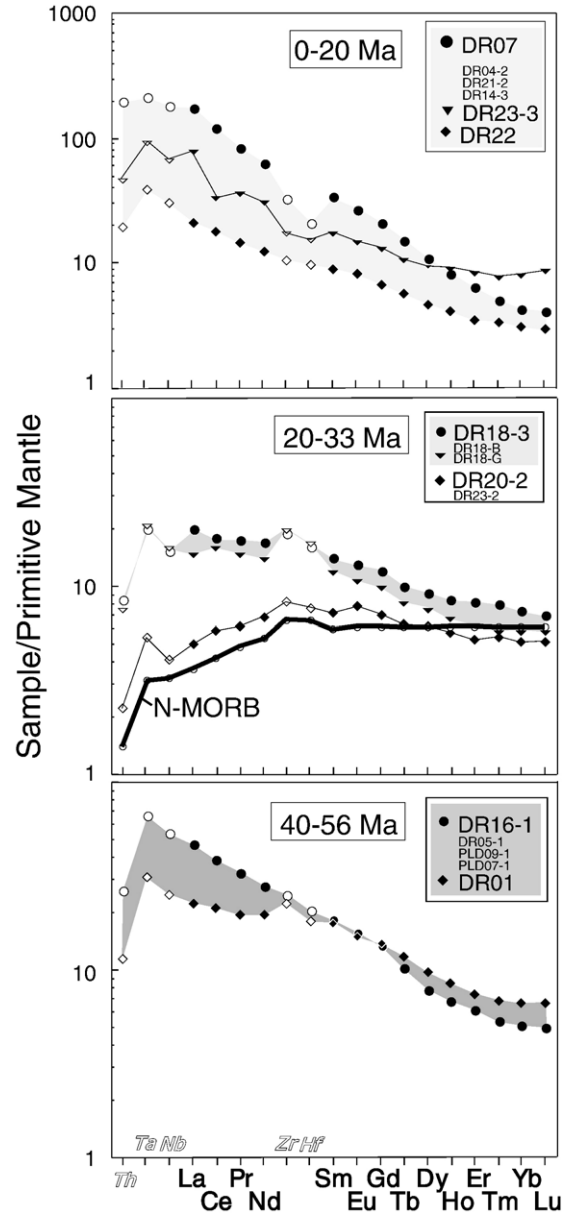
Fig. 6. Primitive-mantle normalized extended rare earth patterns for analyzed samples shown in Table 2. The elements are in decreasing incompatibility order for mantle derived melts. Open symbols are used for non-rare earth elements, Th, Ta, Nb and Zr, Hf [18]. The samples are organized in age groups according to absolute dating or estimated age when italic fonts are used. Grey areas include samples that have similar patterns.

A large range of ages, between 0.23 and 58.1 Ma, is observed with a maximum uncertainty of 2%. These new results bring important constraints to the geodynamical evolution of this region as further discussed in Sections 5 and 6.

4. Geochemical analytical techniques and results

Major, trace element and isotope data are presented in Table 2.

4.1. Sample preparation

Aboard the ship, all samples are crushed to centimeter size fragments. Pieces of glass or chips from the inner part of lava flows or pillow lavas are handpicked to avoid (1) Fe–Mn coatings, which could be a potential source of Pb and Nd contamination and (2) altered surfaces which could have an effect on Sr isotope compositions. All samples (either glasses or rock chips) are washed in an ultrasonic bath of 2 M HCl, followed by double quartz distilled water before further crushing in an agate mortar for major and trace element analysis. For Sr and Nd isotope analyses, the powder is further leached to remove seawater alteration with 0.1 N HCl for a few minutes in an ultrasonic bath and rinsed in deionized water. The Sr–Nd separations are done according to the procedure described in [15]. Pb separation is performed on a separate aliquot of the powdered sample leached with 6 M HCl at 140 °C for an hour and rinsed up to 6 times with deionized water and dried. Such a procedure gives reliable Pb isotope ratios on whole rock powders as shown by Regelous et

al. [16]. Sr and Nd ratios were measured on a Finnigan MAT261 multicollector instrument, in dynamic mode and were corrected for mass fractionation to a value of 8.375209 for $^{88}Sr/^{86}Sr$ and 0.721903 for $^{146}Nd/^{144}Nd$. Standards NBS987, La Jolla and JNdi-1 analyzed during the sample measurement period gave values of 0.71025 ± 2 ($n = 20$), 0.511852 ± 10 ($n = 34$) and 0.512104 ± 4 ($n = 15$). High-resolution Pb analyses were made using the double spike technique with the calibrated Southampton-Brest 207/204 spike [17]. Replicate analyses of the Pb isotope standard NBS981 gave an average of 16.9431 ± 33, 15.5001 ± 39, 36.7317 ± 11 (2sd, $n = 28$) for $^{206}Pb/^{204}Pb$, $^{207}Pb/^{204}Pb$ and $^{208}Pb/^{204}Pb$, respectively. Pb blanks were about 30 pg and thus negligible.

4.2. Major elements

Most samples are alkali basalts and basanites (Fig. 5). Some samples have severe alteration features such as a high loss of ignition. DR14-4 is a basaltic breccia rich in clinopyroxenes.

4.3. Trace elements

The data are presented in Fig. 6. The rare earth diagrams are extended to include Th, Nb, Ta, Zr, Hf and
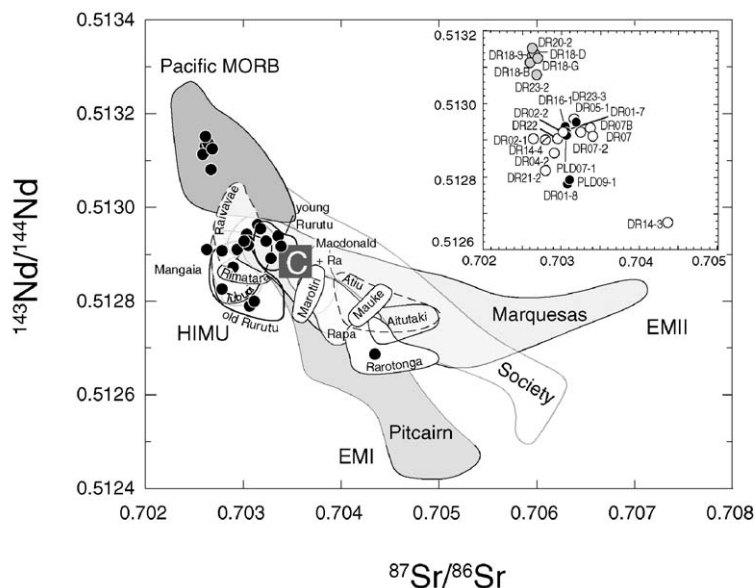

Fig. 7. Nd vs. Sr isotopic diagram for published data from the Austral islands [3,20,29–34] and Marquesas [35–40], Society [33,40] and Pitcairn [41–44] islands as well as Pacific mid-ocean ridge basalts [45–65] and main mantle reservoirs HIMU, EMI and EMII. The numbers in the inset refer to ZEPOLYF2 and POLYDRAG samples. Analytical errors are smaller than symbol sizes. All samples are represented by circles, black for old (40–58 Ma), grey for middle age (20–33 Ma) and white for young (0–20 Ma). DR14-4 dominated by clinopyroxene has a slashed circle as a symbol.
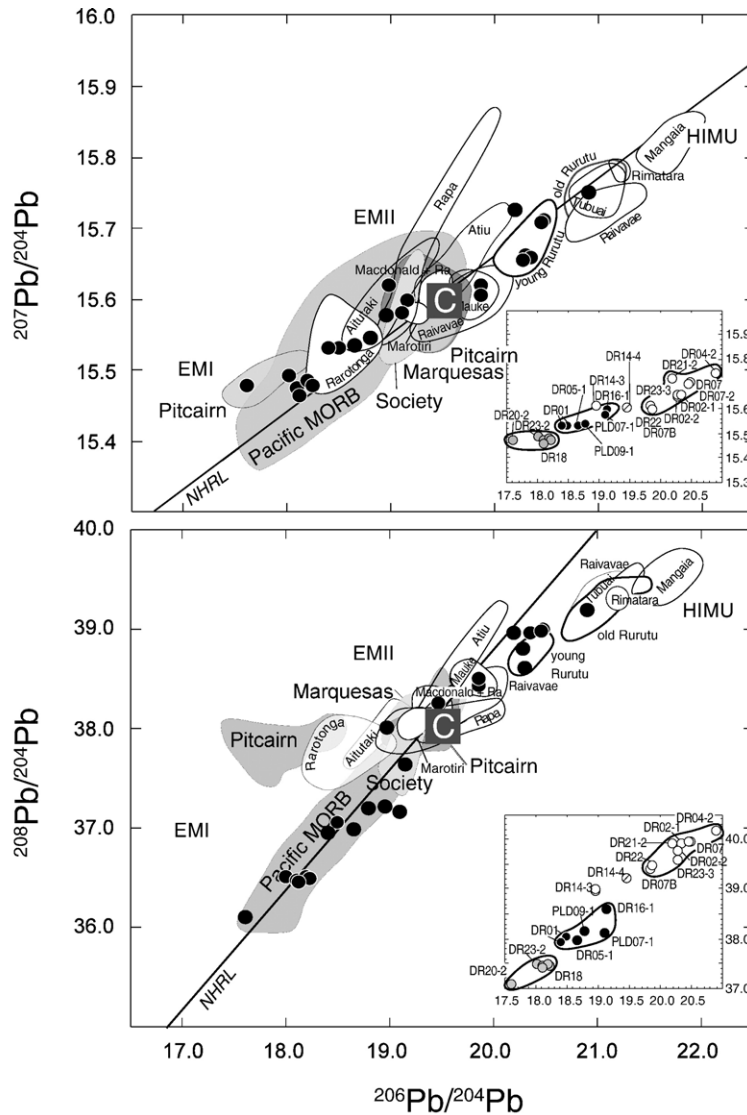
Fig. 8. Pb–Pb diagrams with available data from the literature as specified in Fig. 7 caption and additional references [66–70] for Pacific mid-ocean ridge basalts. NHRL stands for Northern Hemisphere Line [71]. The numbers in the insets refer to ZEPOLYF2 and POLYDRAG samples. Analytical errors are smaller than symbol sizes. Symbols are defined in Fig. 7.

Y. The concentrations are normalized to the primitive mantle values [18], shown in parenthesis after the element name, in Table 2. It is important to note that the samples have been affected by seawater alteration. During such low temperature alteration, however, Nb, Ta, Zr, and Hf remain in the basalt whereas Y and the trivalent REE are partially removed [19]. Therefore concentration ratios of elements such as Zr, Nb, Hf and Ta are considered to be insensitive to alteration. As described above in the sample preparation, more efficient alteration removal has been applied to samples for isotope analyses.

Most samples have light REE enriched patterns, like typical intraplate volcanic lavas (Fig. 6). In detail, however, there seems to be a temporal evolution of the sample patterns. Sample DR14-4, the clinopyroxene rich sample, is not included in this discussion as, due to its low K content, it could not be dated and its extended REE pattern is dominated by clinopyroxenes and thus does not represent the basalt. The oldest group of samples (40–58 Ma) has enrichment in light REE (LREE) relative to heavy REE with $(La/Sm)_N$ between 1.0 and 4.2. The second group (20–33 Ma) has LREE depleted patterns such as found in N-MORB (Normal
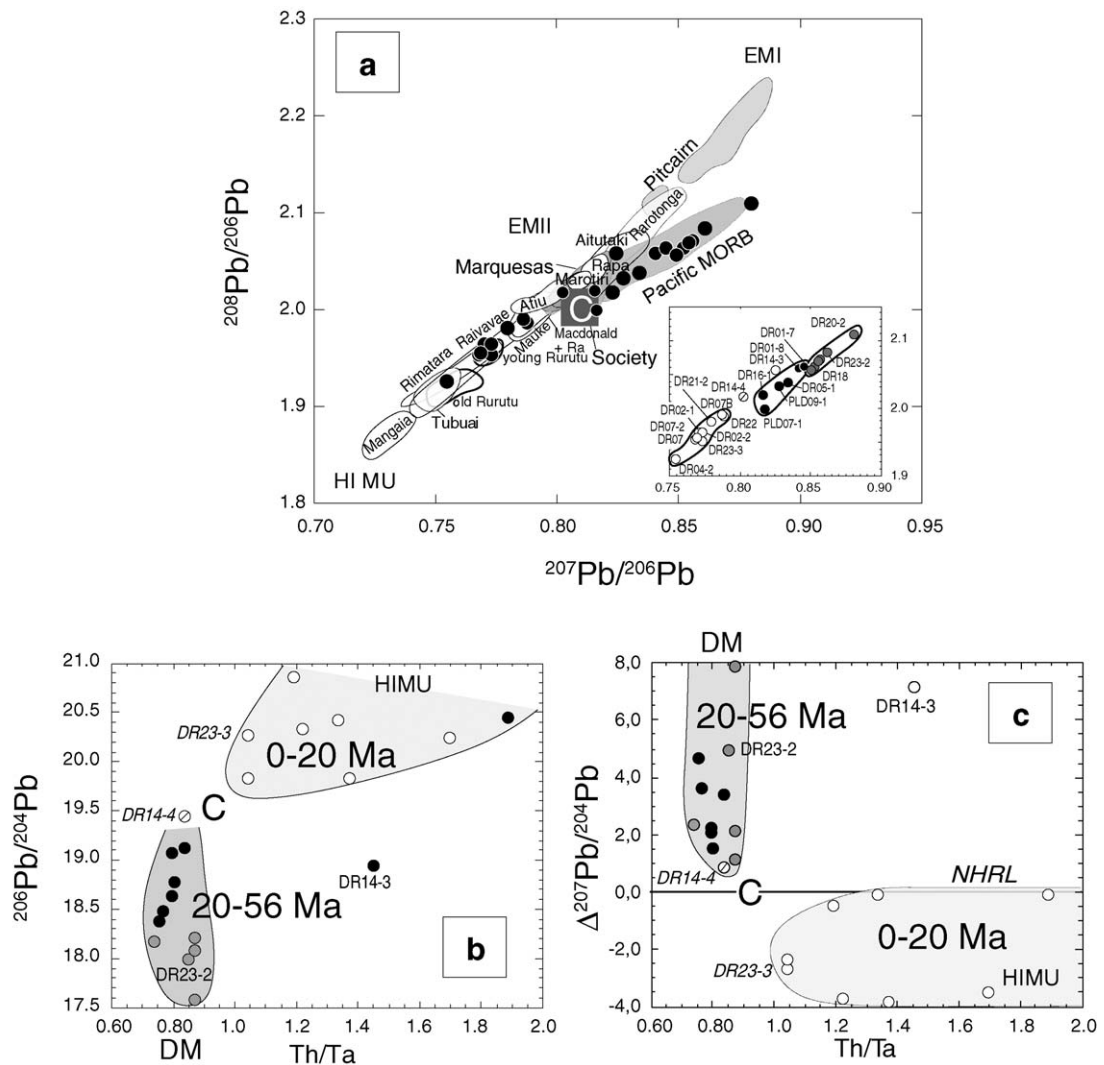
Fig. 9. (a) $^{208}Pb/^{206}Pb$ vs. $^{207}Pb/^{206}Pb$ diagram with available data from the literature as specified in Figs. 7 and 8. (b) $^{206}Pb/^{204}Pb$ and (c) $\Delta^{207}Pb/^{204}Pb$ (deviation from NHRL [71]) versus Th/Ta for studied samples. Symbols are defined in Fig. 7.

Mid-Ocean Ridge Basalts) with $(La/Sm)_N$ between 0.7 and 1.4. The REE patterns of transitional basalts DR20-2 and DR23-2 have negative Nb anomalies and fractionated Nb–Ta and Zr–Hf ratios. Both features are similar to those of depleted MORB basalts. Finally, the youngest group (0–20 Ma) includes LREE patterns as commonly described in intraplate volcanic samples. It shows the largest enrichments and concentration variations of all groups with $(La/Sm)_N$ between 2.2 and 5.0. DR23-3, unfortunately too altered to be dated, is plotted with the youngest group on the basis of its isotopic composition. Although such trace element groupings seem tentative, the isotope data also show similar distinction as is discussed below.

4.4. Isotopes

The isotopic data are not corrected for post-emplacement decay because the Rb/Sr (as can be estimated from the extended REE patterns) and Sm/Nd ratios are small enough that changes in Sr–Nd isotopic ratios are negligible over the considered time period. In the same way, we will assume a negligible evolution of Pb isotopic compositions. The data are therefore compared directly to available data from the literature on samples collected in the same area including Pacific mid-ocean ridge basalt data. All Sr–Nd data from the literature have been normalized to the same standard

values of 0.71025 for NBS987 and 0.511852 for La Jolla.

In all diagrams (Figs. 7–9), the most remarkable feature of the new data is heterogeneity. However it should be remembered that this data set not only includes samples from a wide geographical area but also from a large temporal range (from 58 Ma to present). The values range from very depleted (Sr, Pb) MORB values found in basalts south of the Austral FZ between Rapa and Raivavae (DR18–DR20–DR23) to very radiogenic values. Such depleted MORB-type values (Sr isotopic ratio as low as 0.70258) in intraplate volcanic samples have not been previously reported. The most radiogenic Sr value is found south of the Austral FZ in a basaltic sample (0.70434 — DR14-3). This value is similar to those found in Rarotonga and Aitutaki samples (Fig. 7). Intermediate Sr–Nd values include HIMU-type values similar to those found for Tubuai and Mangaia basalts (DR01–DR04–DR21). Large Sr–Nd isotopic heterogeneity is found within single dredges such as DR14 and DR23. DR14-3 has extreme Sr–Nd compositions towards EM-type mantle sources whereas DR14-4 has Sr–Nd compositions that are close to the HIMU field of compositions. DR23-2 has Sr–Nd isotopic characteristics of Pacific MORB samples whereas DR23-3 has an isotope composition similar to the young volcanic lavas from Rurutu. Examination of Pb–Pb diagrams (Figs. 8 and 9) reinforces these observations. The $^{206}Pb/^{204}Pb$ isotopic compositions display a very wide range, from 17.59 to 20.87. We note that the most depleted samples located on the edge of the Pacific MORB field have higher $^{207}Pb/^{204}Pb$ and $^{208}Pb/^{204}Pb$ ratios than the Northern Hemisphere Regression Line, (NHRL), whereas the most radiogenic samples are located below the NHRL, and are of HIMU-type within the Tubuai–Rimatara field (DR04-2). Other samples have Pb isotopic ratios which vary between Pacific MORB sample values to values typical of those found in Rarotonga–Aitutaki, Macdonald–Raivavae and Rurutu island volcanics (Figs. 8 and 9a). In Fig. 9a, $^{208}Pb/^{206}Pb$ is plotted against $^{207}Pb/^{206}Pb$. We note that the extreme isotopic heterogeneity that was pointed out within a single same dredge is confirmed in Pb–Pb systematics both for DR14 and DR23. Pb–Pb diagrams (Figs. 8 and 9a) suggest that the whole sample set might be divided into three groups according to age: 0–20, 20–33 and 40–58 Ma, consistent with the classification based on the extended rare earth patterns presented above. The youngest group, the most radiogenic in Pb, includes samples with enriched trace element patterns only. The

20–33 Ma age group has MORB isotopic characteristics and includes samples with slightly enriched to depleted XREE patterns. Finally, the 40–58 Ma group includes only trace element enriched samples.

These groups are also clearly separated when a key trace element ratio that is diagnostic of mantle source composition such as Th/Ta (insensitive to variable degrees of partial melting) is combined with Pb isotopic information such as $^{206}Pb/^{204}Pb$ (Fig. 9b) or the distance to the reference line NHRL, $\Delta^{207}Pb/^{204}Pb$ (Fig. 9c). DR14-3, dated at 8.8 Ma, is outside either group as is also shown by its peculiar Nd–Sr isotopic characteristics. A sample with unusual isotopic ratios (Nd composition of 0.51278) was also found in Rurutu Island (74–394) and ignored in the discussion [20]. DR14-4, the clinopyroxene rich basaltic breccia, could not be dated but its geochemical characteristics suggest that it belongs to the 20–33 Ma age group. Samples from a single dredge (DR23) show a very large heterogeneity: $^{206}Pb/^{204}Pb$ ratios vary from 18.0 to 20.3 for DR23-2 and DR23-3, respectively. However DR23-2 is a glassy sample that has been dated at 33 Ma whereas no age is available for DR23-3. These two samples from the same dredge most likely belong to different stages of volcanism. The isotopic characteristics of DR23-3 place it rather in the 0–20 Ma group of samples.

In a Nd vs. Pb isotopic diagram (Fig. 10), the different age groups can also be identified.

5. Discussion

The new geochemical data presented in this paper, based on sampling of seamounts of different ages, clearly illustrate the large heterogeneity of mantle sources at the regional scale of the Cook–Austral island chain between 58 Ma and present.

5.1. Temporal evolution of mantle source composition

This large mantle heterogeneity is seen in isotopes as well as in trace elements. However, the data set appears to be coherent in terms of age, isotope compositions and XREE data:

- Between 58 and 40 Ma, the tapped source presents enriched XREE patterns with a small variation in $^{206}Pb/^{204}Pb$ (18.4–9.0) and with a range in $^{143}Nd/^{144}Nd$ from 0.51280 to 0.51295. This area of the isotopic field is close to what has been referred to as the Common mantle component "C" zone [21] or FOZO (FOcus ZOne) [22] and could represent the
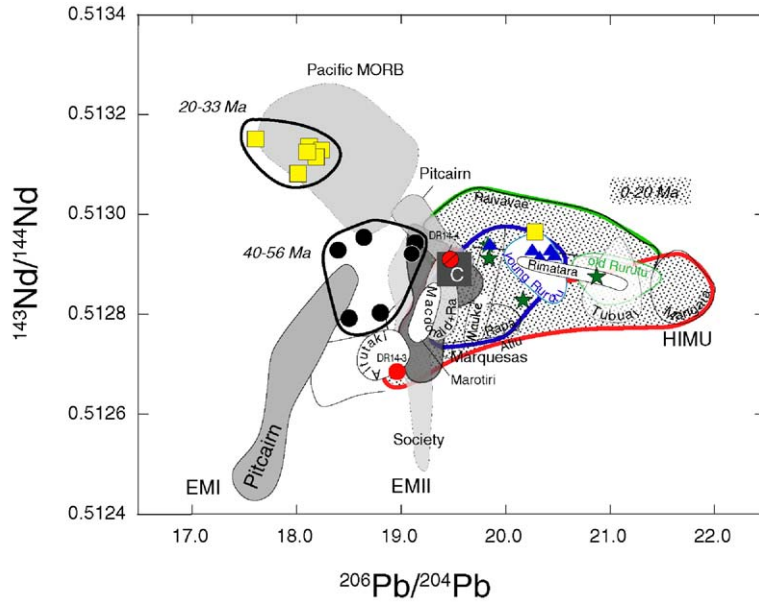
Fig. 10. $^{143}Nd/^{144}Nd$ vs. $^{206}Pb/^{204}Pb$ diagram with available data from the literature as specified in Figs. 7 and 8 captions. Green, blue and red symbols are used for samples belonging to hotspot tracks shown in Fig. 11. Black circles are used for samples dated between 40 and 58 Ma. Yellow squares are used for 33 to 20 Ma samples. The stippled area indicates samples from 0 to 20 Ma.

material found between the enriched blobs in a "marble cake" mantle.

- Between 33 and 20 Ma, the isotopic field describing the source has rather depleted characteristics with almost constant MORB-type Nd values around 0.5131 whereas $^{206}Pb/^{204}Pb$ values range

from 17.6 to 18.2. Samples in this age group present depleted to slightly enriched extended rare earth patterns.

Both groups are characterized by $(La/Sm)_N$ between 0.7 and 4.2 and Th/Ta ratios between 0.7 and 0.9.
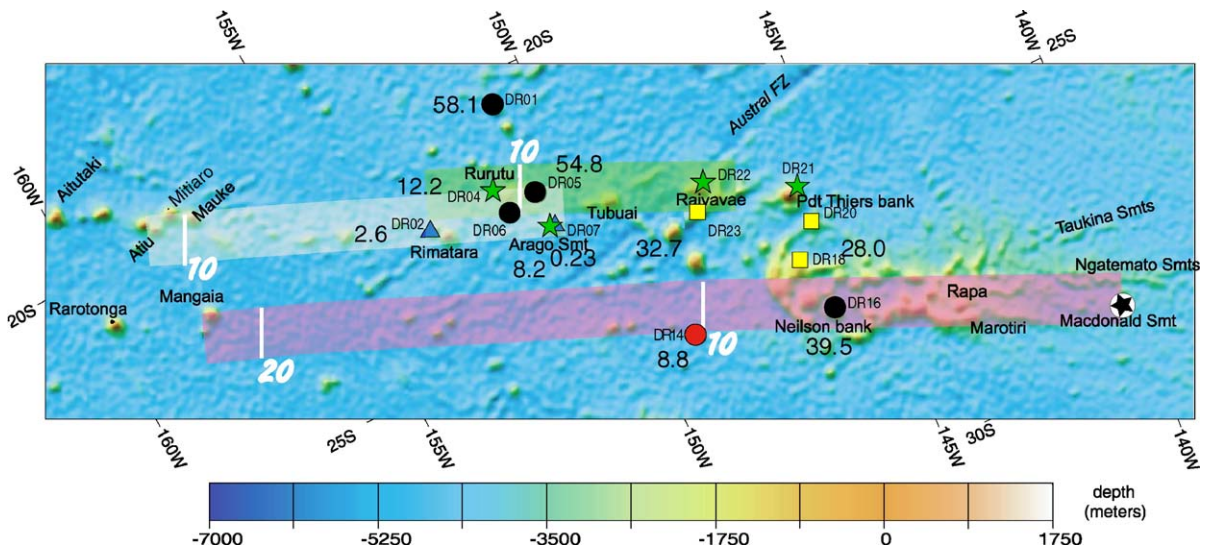
Fig. 11. Bathymetric map with hotspot-track reconstruction for the three groups of volcanoes (see text). Map projection is made along direction of present motion of Pacific plate (from right to left). White italic numbers indicate time in Ma along each track. Note that northernmost track starts at 6.5 Ma for last volcanic event known on this track. A black star represents active Macdonald seamount. The new K–Ar ages obtained in the present study are in black and their exact location are given by the symbols defined in Fig. 10. The known ages of islands are given in Fig. 2.

- Between 20 Ma and present time, the geochemical heterogeneity is larger. The rare earth patterns are the most enriched of all three age groups with (La/Sm)$_N$ between 2.2 and 5.0 and Th/Ta ratios between 1 and 1.9. Isotopically, it is also the most heterogeneous group with $^{206}Pb/^{204}Pb$ ranging from 19.0 to 20.9 and $^{143}Nd/^{144}Nd$ ranging from 0.51269 to 0.51293. In terms of mantle source-types, C to HIMU-types are found. Local heterogeneity can also be observed at the dredge scale, like in DR14 where DR14-3, the only dated sample, and DR14-4 have widely different isotopic ratios. Most likely these two samples are from two different volcanic stages as already pointed out above in the case of DR23.

To summarize, from 58 to 40 Ma, the mantle source is close to C type, between 33 and 20 Ma, the mantle source is of N-MORB-type, between 20 Ma and present time, the source could be a mixture between C and HIMU-type sources. During this last time period, hotspot tracks can be reconstructed.

5.2. Hotspot track reconstruction (0–20 Ma)

Three hotspot tracks have been recognized using a method coupling geodynamical reconstruction and the new K/Ar ages obtained on these samples added to the already available ages on islands.

To reconstruct the apparent path followed by a hotspot on the seafloor, we have moved the hotspot present location back in time by using the set of stage poles proposed by Wessel and Kroenke [23]. This data set represents the most updated synthesis for the absolute Pacific plate motion since 145 Ma. However, for the last interval (0–3 Ma), we have chosen to use the pole previously proposed by Yan and Kroenke [24]. The apparent hotspot tracks are determined for the past 20 m.y. with this set of absolute stage poles (Fig. 11). If we use a 100-km-wide track as representative of the zone of influence of a given hotspot source, we clearly see that the Macdonald hotspot could not have generated the northern Austral Islands. Furthermore, the Macdonald hotspot track fits well with the 19 Ma age of Mangaia and with the K–Ar age of 8.8 Ma obtained on the seamount ZEP2-19 (DR14-3). On the other hand, the northern Austral Islands can be well explained by a hotspot source that probably stopped producing magma at Raivavae ca. 6.5 Ma. This solution has also the advantage of linking together islands with isotopic signatures clearly different from

those of Macdonald. President Thiers bank to the east is a guyot and probably much older. Finally, by using the same stage poles, the Arago track is drawn. It fits quite well with Rurutu and Cook Island ages. Note that volcanoes are often not located along the track axis, which we think emphasizes the importance of lithospheric control over a change in the mantle source location.

5.3. Mantle source variation along hotspot track

When looking at individual hotspot tracks in the last 20 Ma determined above and identified in Fig. 10 with different colors, one can reveal specific characteristics of each of the sources with all tracks including "C" compositions. The three volcanic tracks are from north to south: (1) the Raivavae track (green line and symbols) from Raivavae Island (6.5 Ma) to Rurutu Island and nearby seamounts (12 Ma), (2) the Arago track (blue line and symbols) from Arago Seamount (0.2 Ma) to Atiu Island (8 Ma) and (3) the Macdonald track (red line and symbols) from Macdonald seamount (0 Ma) to Mangaia (19 Ma).

(1) The Raivavae track extends from Raivavae-type (6.5 Ma) to old Rurutu-type (12 Ma) towards the HIMU Mangaia-type. Tubuai Island and DR04-2, a sample dredged on a seamount eastward of Rurutu Island, belong to the old Rurutu field. DR07B, a sample dredged on Arago Seamount, and dated at 8.2 Ma, has a Raivavae signature as well as DR22, a sample dredged on the northeast flank of Raivavae Island. If we extend the track eastward in order to find the youngest event, we find President Thiers guyot where DR21 was collected. Its isotopic signature is not far from that of the Raivavae field but only a radiometric age will settle the question.

(2) The Arago (DR7) track appears more homogeneous and could be related to the young Rurutu volcanic episode (1 Ma). Along this track, DR2 (2.6 Ma), a sample dredged on a seamount westward of Rimatara Island, has the same signature. Rimatara Island samples, although dated at 27 Ma [8], are clearly belonging to the Young Rurutu episode. The Rimatara Island is thus likely belonging to this track and we think that the existing radiometric age already questioned by several authors is definitively an error. At the oldest end of the track, Atiu and Mauke have less radiogenic Nd isotopes and their belonging to the track is thus more questionable,

although one Mauke sample is close to the young Rurutu field.

(3) The Macdonald track source is more heterogeneous than the other tracks, at the scale of the track as well as at the scale of each volcano. The volcano scale heterogeneity is seen especially in Nd isotopes in samples from Macdonald, Rapa, Marotiri and DR14-3, dated at 8.8 Ma. The track heterogeneity is illustrated by the difference in isotopic signature between Macdonald (0 Ma) and Mangaia whose age (19 Ma) is in agreement with the age along the track.

From the above description of mantle isotopic characteristics associated with each of these three hotspot tracks, it can be deduced that the mantle tapped in the last 20 Ma is more radiogenic and more heterogeneous than earlier. Further detailed work on identifying the different volcanic episodes present in the different volcanoes in correlation with basement ages would be needed to raise reasonable hypotheses about the causes of such heterogeneities. We certainly can assume that the superplume mantle source was heterogeneous to start with 20 Ma ago. And we can safely state that mixing of sources combined with crustal assimilation would increase the observed degree of heterogeneity within each hotspot track.

5.4. Lithospheric control

As described earlier, geochemical heterogeneities are present even at the scale of a single volcano. On some island or seamount, important differences in geochemical signatures can be pointed out. These signatures however clearly belong to different volcanic stages separated in time by several millions of years. This is well known on Rurutu Island [25] with two stages dated at 12 Ma (old Rurutu stage) and 1 Ma (Young Rurutu stage). Furthermore, if we consider the nearby Lotus bank with a sample dated at 54.8 Ma, we can conclude that at least three different stages have occurred in the same area. The present study also reveals that Arago Seamount experienced two volcanic stages separated by 8.7 m.y. (DR7 and DR7b samples) with distinct isotopic signatures. On the other hand, DR14 and DR23 samples are presenting different isotopic signatures but we don't know their difference in ages. We can therefore assume that each of them has sampled two separate episodes of volcanism in the same way as two volcanic stages have been identified in Rurutu Island or Arago Seamount. During such a time interval (around 10 m.y.), the Pacific plate has moved 1200 km to the Northwest and the volcanic activity cannot correspond to the same mantle source. To explain such reoccurrence of volcanism at the same location, we have to assume that the lithosphere is weakened along the path taken by the magma to reach the surface. This weakened area then acts as the preferential pathway for subsequent magmatic events that bring magma from new plume sources to the surface.

6. Conclusion

Based on the most complete to date oceanic sampling of the Cook–Austral volcanic chains, we have shown:

- a huge heterogeneity in mantle sources at the regional scale;
- a chemical grouping of the mantle sources during the three identified volcanic stages of 58–40, 33–20 and 20–0 Ma with signatures of mantle reservoir composition from close to C to N-MORB-types and C/HIMU-type, respectively.
- a mantle heterogeneity along each hotspot track during the most recent volcanic period of 0–20 Ma;
- an heterogeneity at the scale of a volcano due to the occurrence of different magmatic phases at the same location;
- the importance of the structural control, either crustal or lithospheric, in the location of magma outputs.

These observations taken together are in good agreement with a model where each hotspot could sample one volume of the large and very heterogeneous plume responsible for the regional swell of the seafloor topography [1]. It has been proposed that this small scale convection (100 km in surface expression compared to the 2000 km of the Superswell) could be due to secondary instabilities developing at the surface of the larger plume in the transition zone [26]. The time constants of these phenomena should give us constraints to infer the size of the mantle heterogeneities described in this study. At the regional scale, the challenge is to decipher the dynamics of the super-plume responsible for the Superswell, given the time evolution of the mantle source composition.

Acknowledgments

References

[1] M.K. McNutt, K.M. Fischer, The South Pacific Superswell, in: B. Keating, P. Fryer, R. Batiza, G. Boethlert (Eds.), Seamounts, Islands and Atolls, Geophys. Monogr., vol. 43, AGU, Washington D.C., 1987, pp. 25–34.

[2] H. Staudigel, K.-H. Park, M. Pringle, J.L. Rubenstone, W.H.F. Smith, A. Zindler, The longevity of the South Pacific isotopic and thermal anomaly, Earth Planet. Sci. Lett. 102 (1991) 24–44.

[3] P. Schiano, K.W. Burton, B. Dupre, J.L. Birck, G. Guille, C.J. Allegre, Correlated Os–Pb–Nd–Sr isotopes in the Austral–Cook chain basalts: the nature of mantle components in plume sources, Earth Planet. Sci. Lett. 186 (2001) 527–537.

[4] V. Clouard, A. Bonneville, P.Y. Gillot, The Tarava seamounts: a new but extinct hotspot chain on the South Pacific Superswell, Earth Planet. Sci. Lett. 207 (2003) 117–130.

[5] C.L. Mayes, L.A. Lawver, D.T. Sandwell, Tectonic history and new isochron chart of the South Pacific, J. Geophys. Res. 95 (B6) (1990) 8543–8567.

[6] M.K. McNutt, D.W. Caress, J. Reynolds, K.A. Jordahl, R.A. Duncan, Failure of plume theory to explain midplate volcanism in the Southern Austral islands, Nature 389 (1997) 479–482.

[7] N. Baudry, U. Von Stackelberg, J. Récy, Alignements volcaniques dans les iles Australes: analyse et interprétation des données SEASAT et Seabeam, C. R. Acad. Sci. — Paris 306 (Série II) (1988) 643–648.

[8] D.L. Turner, R.D. Jarrard, K/Ar dating of the Cook Austral island chain; a test of the hot spot hypothesis, J. Volcanol. Geotherm. Res. 12 (1982) 187–220.

[9] H. Barsczus, G. Guille, R.C. Maury, C. Chauvel, H. Guillou, Two magmatic sources at Rurutu Island (Austral Islands, French Polynesia) and the Austral "hotline", Eos, Trans. A. G. U. 75 (16 Suppl.) (1994) 323.

[10] A. Bonneville, R. Le Suavé, L. Audin, V. Clouard, L. Dosso, P.-Y. Gillot, P. Janney, A. Jordahl Kelsey, K. Maamaatuaiahutapu, Arago Seamount: the missing hot spot found in the Austral Islands, Geology 30 (11) (2002) 1023–1026.

[11] G.B. Dalrymple, M.A. Lanphere, Potassium–argon dating, Principles, Techniques and Applications to Geochronology, W. H. Freeman and Co., San Francisco, 1969, 258 pp.

[12] P.Y. Gillot, Y. Cornette, The Cassignol technique for potassium–argon dating, precision and accuracy: examples from late Pleistocene to recent volcanics from southern Italy, Chem. Geol. 59 (1986) 205–222.

[13] I. McDougall, T.M. Harrison, Geochronology and Thermochronology by the $^{40}Ar/^{39}Ar$ Method, Oxford University Press, New York, 1999, 269 pp.

[14] C. Cassignol, P.Y. Gillot, Range and effectiveness of unspiked potassium–argon dating: experimental groundwork and applications, in: G.S. Odin (Ed.), Numerical Dating in Stratigraphy, Wiley, Chichester, 1982, pp. 159–179.

[15] L. Dosso, H. Bougault, J.L. Joron, Geochemical morphology of the North Mid-Atlantic Ridge, 10°–24°N: trace element–isotopes complementarity, Earth Planet. Sci. Lett. 120 (1993) 443–462.

[16] M. Regelous, A.W. Hofmann, W. Abouchami, S.J.G. Galer, Geochemistry of lavas from the Emperor Seamounts, and the geochemical evolution of Hawaiian magmatism from 85 to 42 Ma, J. Petrol. 44 (1) (2003) 113–140.

[17] O. Ishizuka, R.N. Taylor, J.A. Milton, R.W. Nesbitt, Fluid-mantle interaction in an intra-oceanic arc: constraints from high-precision Pb isotopes, Earth Planet. Sci. Lett. 211 (2003) 221–236.

[18] S.S. Sun, W.F. McDonough, Chemical and isotopic systematics of oceanic basalts: implications for mantle composition and processes, in: A.D. Saunders, M.J. Norry (Eds.), Magmatism of the Ocean Basins, vol. 42, Geol. Soc. Spec. Publication, 1989, pp. 313–345.

[19] P. Bienvenu, H. Bougault, J.L. Joron, M. Treuil, L. Dmitriev, MORB alteration : rare-earth element/non rare-earth hygromagmaphile element fractionation, Chem. Geol. 82 (1990) 1–14.

[20] C. Chauvel, W. McDonough, G. Guille, R. Maury, R. Duncan, Contrasting old and young volcanism in Rurutu Island, Austral Chain, Chem. Geol. 139 (1–4) (1997) 125–143.

[21] B.B. Hanan, D.W. Graham, Lead and helium isotope evidence from Oceanic Basalts for a common deep source of mantle plumes, Science 272 (1996) 991–995.

[22] S.R. Hart, E.H. Hauri, L.A. Oschmann, J.A. Whitehead, Mantle plumes and entrainment: isotopic evidence, Science 256 (1992) 517–520.

[23] P. Wessel, L. Kroenke, A geometric technique for relocating hotspots and refining absolute plate motions, Nature 387 (1997) 365–369.

[24] C.Y. Yan, L.W. Kroenke, A plate tectonic reconstruction of the Southwest Pacific, 0–100 Ma, Proceedings of the Ocean Drilling Project, Scientific Results, vol. 130, 1993, pp. 697–709.

[25] R.A. Duncan, W. Compston, Sr isotopic evidence for an old mantle source region for French Polynesian volcanism, Geology 4 (1976) 728–732.

[26] A. Davaille, Simultaneous generation of hotspots and superswells by convection in a heterogeneous planetary mantle, Nature 402 (1999) 756–760.

[27] R.W. Le Maitre, P. Bateman, A. Dudek, J. Keller, M.J.L.L. Bas, P.A. Sabine, R. Schmid, H. Sorensen, A. Streckeisen, A.R. Woolley, B. Zanettin, A Classification of Igneous Rocks and Glossary of Terms, Blackwell Scientific Publications, Oxford, 1989, 193 pp.

[28] G.A. MacDonald, T. Katsura, Chemical composition of Hawaiian lavas, J. Petrol. 5 (1964) 83–133.

[29] Y. Nakamura, M. Tatsumoto, Pb, Nd, and Sr isotopic evidence for a multicomponent source for rocks of Cook–Austral Islands and heterogeneities of mantle plumes, Geochim. Cosmochim. Acta 52 (12) (1988) 2909–2924.

[30] Z.A. Palacz, A.D. Saunders, Coupled trace element and isotope enrichment in the Cook–Austral–Samoa islands, southwest Pacific, Earth Planet. Sci. Lett. 79 (1986) 270–280.

[31] E.H. Hauri, S.R. Hart, Re Os isotope systematics of HIMU and EMII oceanic island basalts from the South Pacific Ocean, Earth Planet. Sci. Lett. 114 (1993) 353–371.

[32] T. Kogiso, Y. Tatsumi, G. Shimoda, H.G. Barsczus, High μ (HIMU) ocean Island Basalts in Southern Polynesia: new

evidence for whole mantle scale recycling of subducted oceanic crust, J. Geophys. Res. 102 (B4) (1997) 8085–8103.

[33] C. Hemond, C.W. Devey, C. Chauvel, Source compositions and melting processes in the Society and Austral plumes (South Pacific Ocean); element and isotope (Sr, Nd, Pb, Th) geochemistry, Chem. Geol. 115 (1994) 7–45.

[34] J.D. Woodhead, Extreme HIMU in an oceanic setting; the geochemistry of Mangaia Island (Polynesia), and temporal evolution of the Cook–Austral hotspot, J. Volcanol. Geotherm. Res. 12 (3–4) (1996) 187–220.

[35] D.L. Desonie, R.A. Duncan, J.H. Natland, Temporal and geochemical variability of volcanic products of the Marquesas hotspot, J. Geophys. Res. 98 (1993) 17,649–17,665.

[36] J.M. Liotard, H.G. Barsczus, C. Dupuy, J. Dostal, Geochemistry and origin of basaltic lavas from Marquesas Archipelago, French Polynesia, Contrib. Mineral. Petrol. 92 (1986) 260–268.

[37] R.A. Duncan, M.T. Mc Culloch, H.G. Barsczus, D.R. Nelson, Plume versus lithospheric sources for melts at Ua Pou, Marquesas Islands, Nature 322 (1986) 534–538.

[38] P. Vidal, C. Chauvel, R. Brousse, Large mantle heterogeneity beneath French Polynesia, Nature 307 (1984) 536–538.

[39] J.D. Woodhead, Temporal geochemical evolution in oceanic intra-plate volcanics; a case study from the Marquesas (French Polynesia) and comparison with other hotspots, Contrib. Mineral. Petrol. 111 (1992) 458–467.

[40] Q.C. Cheng, J.D. Macdougall, G.W. Lugmair, Geochemical studies of Tahiti, Teahitia and Mehetia, Society Island Chain, J. Volcanol. Geotherm. Res. 55 (1993) 155–184.

[41] J.D. Woodhead, C.W. Devey, Geochemistry of the Pitcairn Seamounts. 1. Source character and temporal trends, Earth Planet. Sci. Lett. 116 (1993) 81–99.

[42] J.D. Woodhead, M.T. McCulloch, Ancient seafloor signals in Pitcairn Island lavas and evidence for large amplitude, small length-scale mantle heterogeneities, Earth Planet. Sci. Lett. 94 (1989) 257–273.

[43] C. Dupuy, P. Vidal, R.C. Maury, G. Guille, Basalts from Mururoa, Fangataufa and Gambier islands (French Polynesia); geochemical dependence on the age of the lithosphere, Earth Planet. Sci. Lett. 117 (1993) 89–100.

[44] J. Eisele, M. Sharma, S.J.G. Galer, J. Blichert-Toft, C.W. Devey, A.W. Hofmann, The role of sediment recycling in EM-1 inferred from Os, Pb, Hf, Nd, Sr isotope and trace element systematics of the Pitcairn hotspot, Earth Planet. Sci. Lett. 196 (2002) 197–212.

[45] W.M. White, A.W. Hofmann, H. Puchelt, Isotope geochemistry of Pacific Mid-Ocean ridge basalt, J. Geophys. Res. 92 (B6) (1987) 4881–4893.

[46] J.J. Mahoney, J.M. Sinton, M.D. Kurz, J.D. Macdougall, K.J. Spencer, G.W. Lugmair, Isotope and trace element characteristics of a super-fast spreading ridge: East Pacific rise, 13–23°S, Earth Planet. Sci. Lett. 121 (1994) 173–193.

[47] Y.L. Niu, D.G. Waggoner, J.M. Sinton, J.J. Mahoney, Mantle source heterogeneity and melting processes beneath seafloor spreading centers: the East Pacific Rise, 18 degrees-19S, J. Geophys. Res. 101 (B12) (1996) 27711–27733.

[48] W. Bach, E. Hegner, J. Erzinger, M. Satir, Chemical and isotopic variations along the superfast spreading East Pacific rise from 6 degrees S to 30 degrees S, Contrib. Miner. Petrol. 116 (4) (1994) 365–380.

[49] J.D. Macdougall, G.W. Lugmair, Sr and Nd isotopes in basalts from the East Pacific Rise: significance for mantle heterogeneity, Earth Planet. Sci. Lett. 77 (1986) 273–284.

[50] E. Ito, W.M. White, C. Göpel, The O, Sr, Nd and Pb isotope geochemistry of MORB, Chem. Geol. 62 (1987) 157–176.

[51] W.M. White, A.W. Hofmann, Sr and Nd isotope geochemistry of oceanic basalts and mantle evolution, Nature 296 (1982) 821–825.

[52] R.S. Cohen, N.M. Evensen, P.J. Hamilton, R.K. O'Nions, U–Pb, Sm–Nd and Rb–Sr systematics of mid-ocean ridge basalt glasses, Nature 283 (1980) 149–153.

[53] R.S. Cohen, R.K. O'Nions, The lead, neodymium and strontium isotopic structure of ocean ridge basalts, J. Petrol. 23 (1982) 299–324.

[54] E. Hegner, M. Tatsumoto, Pb, Sr, and Nd isotopes in basalts and sulfides from the Juan de Fuca Ridge, J. Geophys. Res. 92 (1987) 11380–11386.

[55] A. Prinzhofer, E. Lewin, C.J. Allègre, Stochastic melting of the marble cake mantle: evidence from local study of the East Pacific Rise at 12°50′N, Earth Planet. Sci. Lett. 92 (1989) 189–206.

[56] P. Schiano, J.L. Birck, C.J. Allegre, Osmium–strontium–neodymium–lead isotopic covariations in mid-ocean ridge basalt glasses and the heterogeneity of the upper mantle, Earth Planet. Sci. Lett. 150 (1997) 363–379.

[57] S.P. Verma, J.G. Schilling, D.G. Waggoner, Neodynium isotopic evidence for Galapagos hotspot-spreading centre system evolution, Nature 306 (1983) 654–657.

[58] W. Bach, J. Erzinger, L. Dosso, C. Bollinger, H. Bougault, J. Etoubleau, J. Sauerwein, Unusually large Nb–Ta depletions in North Chile ridge basalts at 36 degrees 50′ to 38 degrees 56′S: major element, trace element, and isotopic data, Earth Planet. Sci. Lett. 142 (1996) 223–240.

[59] E.M. Klein, J.L. Karsten, Ocean-ridge basalts with convergent-margin geochemical affinities from the Chile Ridge, Nature 374 (1995) 52–57.

[60] J.D. Macdougall, G.W. Lugmair, Extreme isotopic homogeneity among basalts from the southern East Pacific Rise: mantle or mixing effect? Nature 313 (1985) 209–211.

[61] P.R. Castillo, J. Natland, Y. Niu, P.F. Lonsdale, Sr, Nd and Pb isotopic variation along the Pacific-antarctic risecrest, 53–57°S: implications for the composition and dynamics of the South Pacific upper mantle, Earth Planet. Sci. Lett. 154 (1998) 109–125.

[62] E.M. Ferguson, E.M. Klein, Fresh basalts from the Pacific Antarctic ridge extend the pacific geochemical province, Nature 366 (1993) 330–333.

[63] D.G. Pyle, D.M. Christie, J.J. Mahoney, Resolving an isotopic boundary within the Australian–Antarctic discordance, Earth Planet. Sci. Lett. 112 (1992) 161–178.

[64] E.M. Klein, C.H. Langmuir, A. Zindler, H. Staudigel, B. Hamelin, Isotope evidence of a mantle convection boundary at the Australian–Antarctic discordance, Nature 333 (1988) 623–629.

[65] I. Vlastelic, L. Dosso, H. Bougault, D. Aslanian, L. Geli, J. Etoubleau, M. Bohn, J.L. Joron, C. Bollinger, Chemical systematics of an intermediate spreading ridge: the Pacific–Antarctic ridge between 56 degrees S and 66 degrees S, J. Geophys. Res. Solid Earth 105 (B2) (2000) 2915–2936.

[66] B. Dupré, B. Lambret, D. Rousseau, C.J. Allègre, Limitations on the scale of mantle heterogeneities under oceanic ridges, Nature 294 (1981) 552–554.

[67] S.E. Church, M. Tatsumoto, Lead isotope relations in oceanic ridge basalts from the Juan de Fuca-Gorda Ridge area, N.E. Pacific Ocean, Contrib. Mineral. Petrol. 53 (1975) 253–279.

[68] S.S. Sun, Lead isotopic study of young volcanic rocks from mid-ocean ridges, ocean islands and island arcs, Philos. Trans. R. Soc. Lond., A 297 (1980) 409–445.

[69] D. Fontignie, J.-G. Schilling, $^{87}Sr/^{86}Sr$ and REE variations along the Easter Microplate boundaries (south Pacific): application of multivariate statistical analyses to ridge segmentation, Chem. Geol. 89 (1991) 209–241.

[70] B.B. Hanan, J.-G. Schilling, Easter microplate evolution: Pb isotope evidence, J. Geophys. Res. 94 (1989) 7432–7448.

[71] S.R. Hart, A large scale isotope anomaly in the Southern Hemisphere mantle, Nature 309 (1984) 753–757.